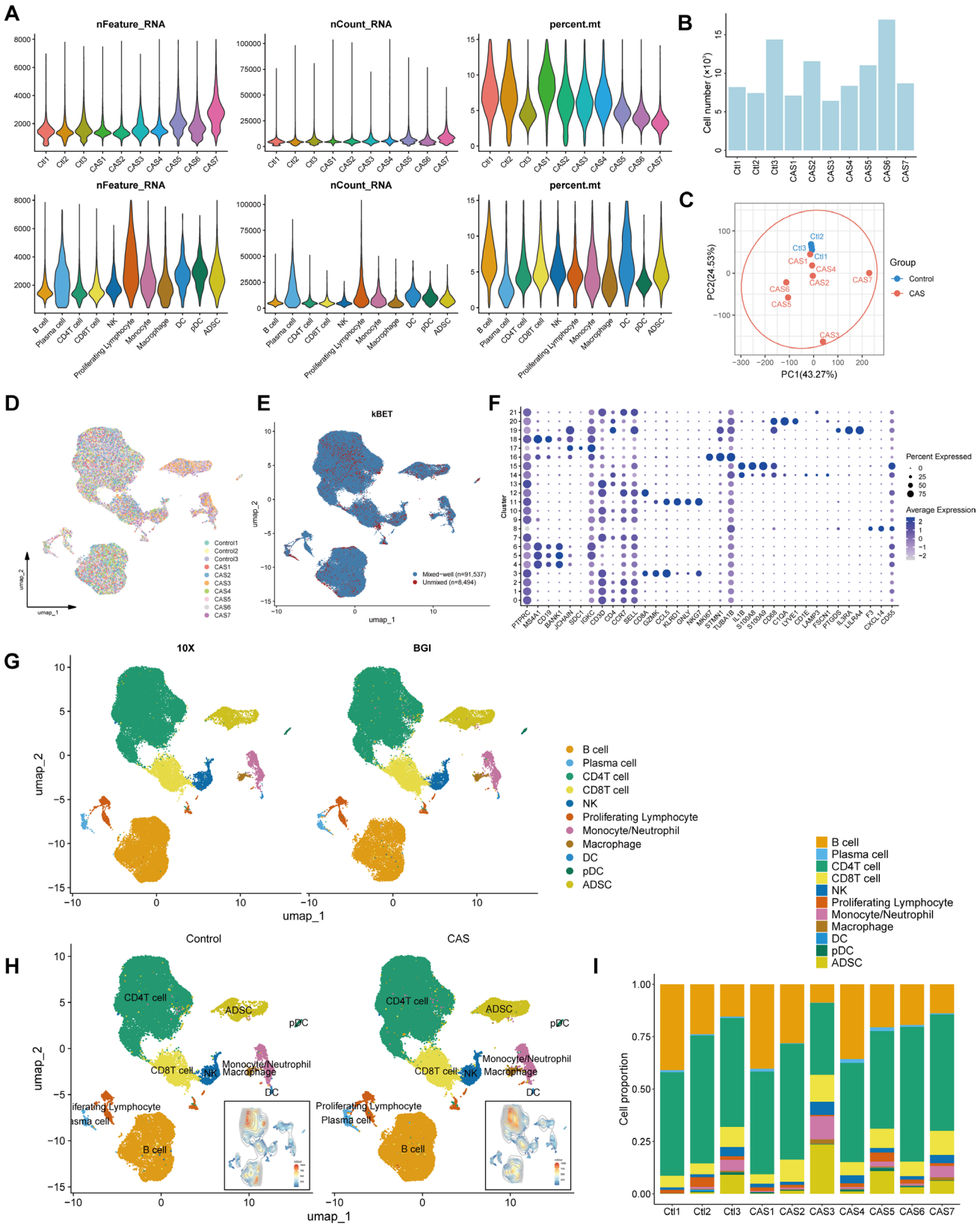
Supplementary Materials

Perivascular Adipose Single-Cell Atlas Identifies CD55^{+} Adipose-derived Stem Cells as Vascular Remodeling Regulators in Atherosclerosis

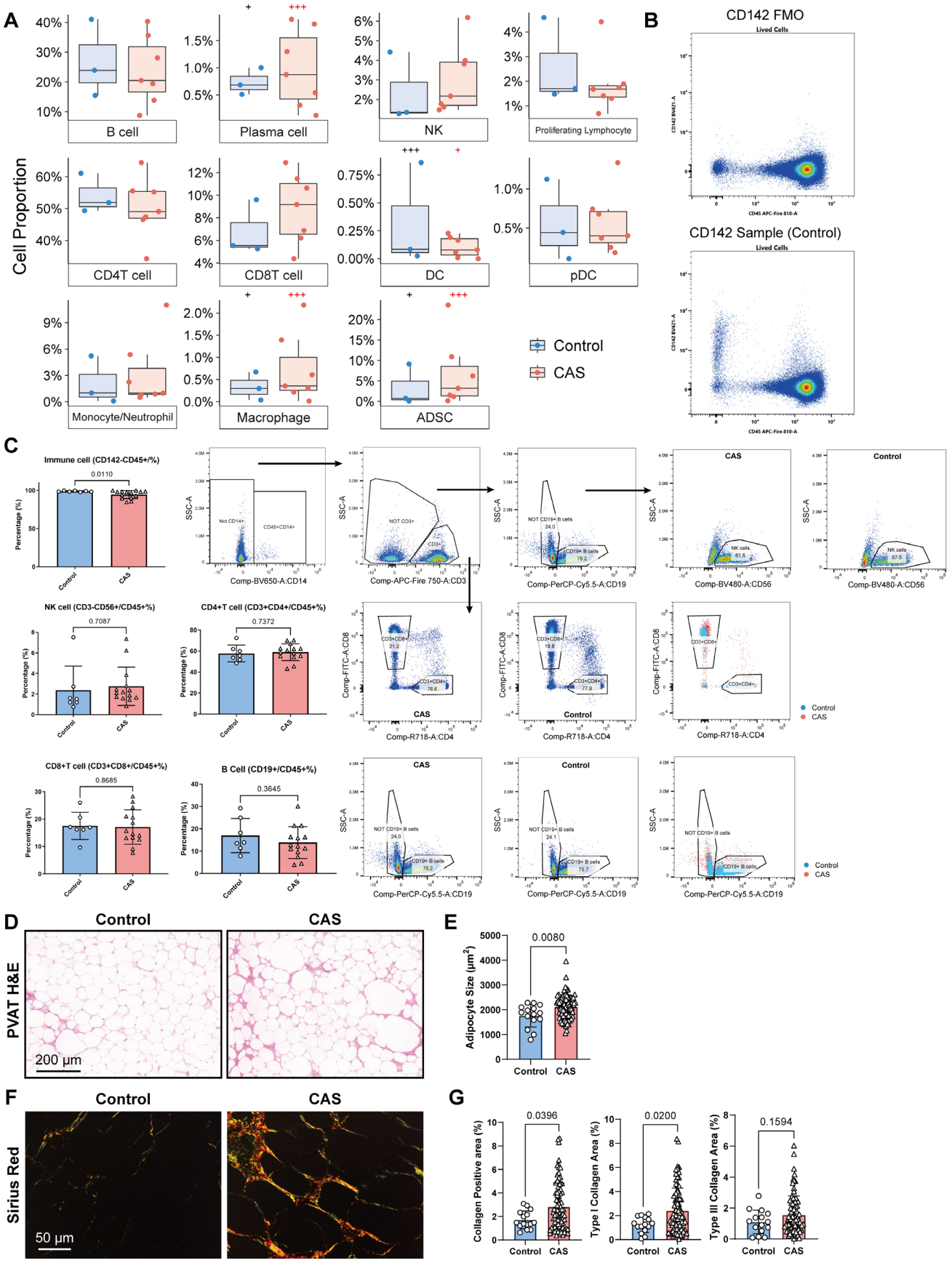
Junye Chen[1,2#], Kang Li[1#], Jiang Shao[1#], Song Mei[3#], Zhichao Lai[1#], Hongmei Zhao[2,4], Xiaohan Duan[1], Yunfei Xue[2], Xingqi Xiao[2], Yuyao Feng[1], Zhiwei Li[2], Zhan Zhu[1,5], Keqiang Shu[1], Deqiang Kong[1], Yiyun Xie[1], Leyin Xu[1], Chaonan Wang[1], Yanan Liu[1], Ziyan Xie[6], Yixuan Huang[7], Xinlei Zhang[7], Jing Wang[2,8]*, Peng Zhang[9]*, Bao Liu[1,10,11]*

[1]Department of Vascular Surgery, Peking Union Medical College Hospital, Peking Union Medical College and Chinese Academy of Medical Sciences, Beijing, China;
[2]Department of Pathophysiology, Institute of Basic Medical Sciences, Chinese Academy of Medical Sciences and Peking Union Medical College, Beijing, China;
[3]Institute of Blood Transfusion, Chinese Academy of Medical Sciences and Peking Union Medical College, Chengdu, China;
[4]State Key Laboratory of Complex, Severe, and Rare Diseases, Beijing, China;
[5]Jiangxi Provincial People's Hospital, Nanchang Medical College, Nanchang, China;
[6]Department of Radiology, Peking Union Medical College Hospital, Peking Union Medical College and Chinese Academy of Medical Sciences, Beijing, China;
[7]Beijing Geneworks Technology Co., Ltd. Beijing, China;
[8]State Key Laboratory of Respiratory Health and Multimorbidity, Beijing, China;
[9]Beijing Pediatric Research Institute, Beijing Children's Hospital, Capital Medical University, Beijing, China.
[10]Institute of Aging and Health, Chinese Academy of Medical Sciences, Beijing, China.
[11]School of Aging and Health, Peking Union Medical College, Beijing, China.
[#]These authors contributed equally.
[*]Corresponding authors.



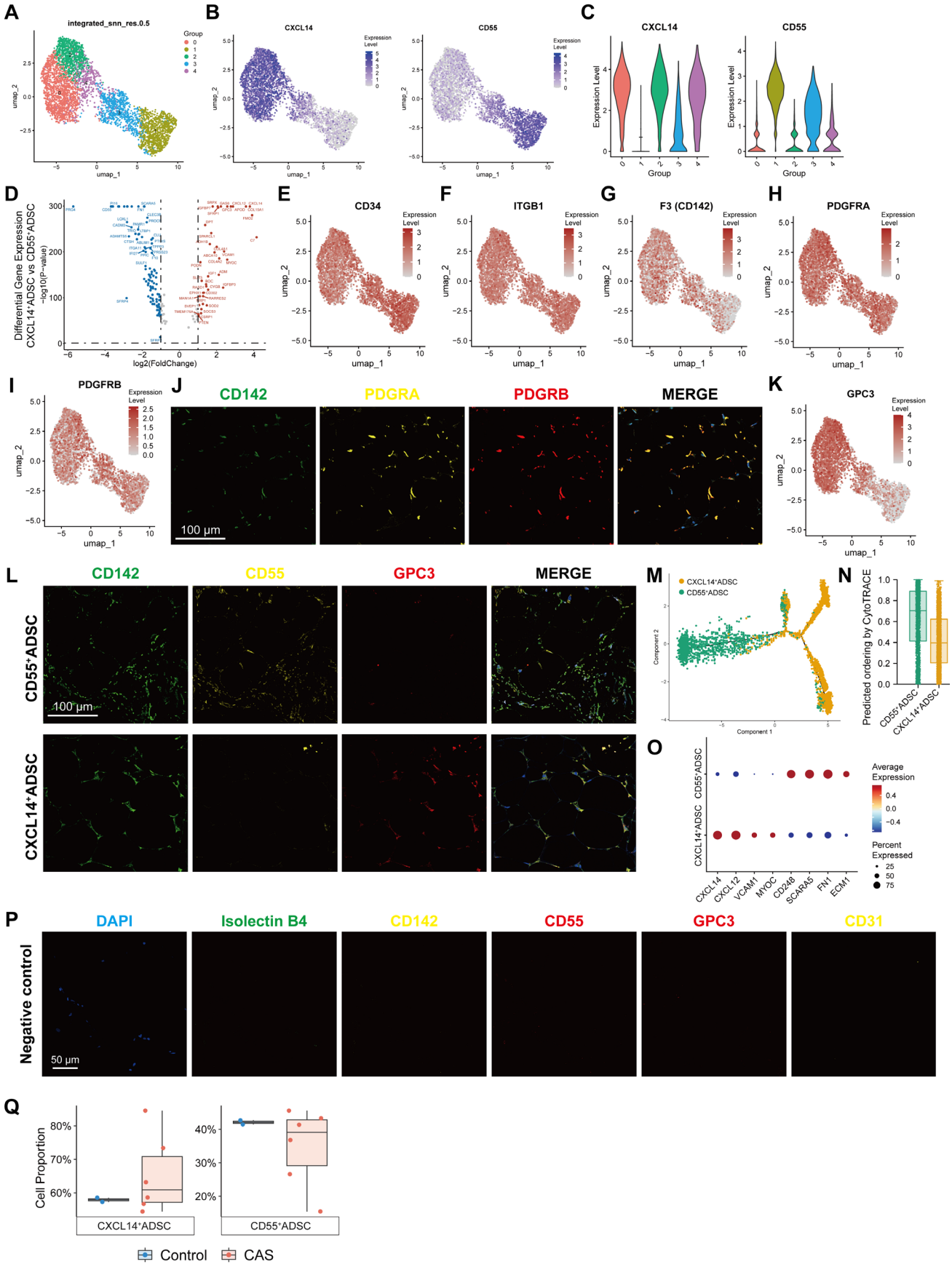
Supplementary figure 1. Single-cell transcriptomic analysis of PVAT from patients with carotid stenosis. (A) Quality control metrics for PVAT scRNA-seq data across samples and annotated cell

types. **(B)** Single-cell capture yield across PVAT sample. **(C)** Separation trend of all PVAT scRNA-seq data evaluated by principal component analysis (PCA). **(D)** UMAP plots of the scRNA-seq profiles from each sample after batch effect correction. **(E)** Evaluation of the effectiveness of batch effect removal using the kBET method. **(F)** Dot plot of the expression of canonical markers for identified clusters. **(G)** UMAP embeddings stratified by sequencing platform (10x Genomics and DNBelab, BGI). **(H)** UMAP plots and density plots of the scRNA-seq profiles stratified by control group and CAS group. **(I)** Histogram displaying the proportion of each major cell type of all samples. PVAT: perivascular adipose tissue; CAS: carotid stenosis; UMAP: uniform manifold approximation and projection; ADSC: adipose-derived stem cell; BGI: Beijing Genomics Institute. Source data are provided as a Source Data file.



Supplementary figure 2. Cellular compositional shifts and fibrotic features in PVAT from

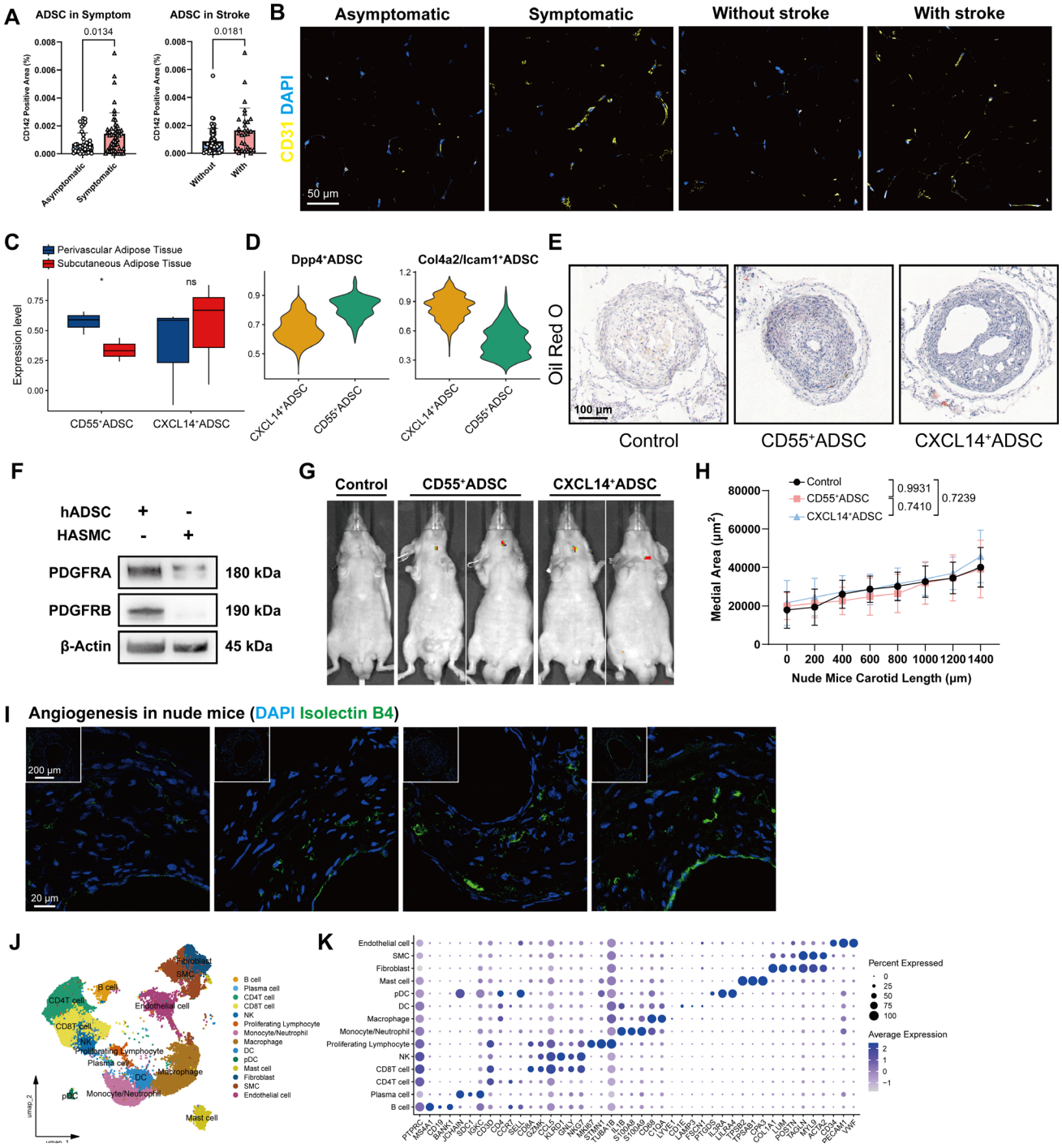
patients with carotid atherosclerosis. (A) Box plot of the proportion of major cell types in CAS v.s. control groups. The differences between groups with a magnitude of ++ are presented. +++, Ro/e > 1; ++, 0.8 < Ro/e ≤ 1; +, 0.2 ≤ Ro/e ≤ 0.8; +/−, 0 < Ro/e < 0.2; −, Ro/e = 0; in which Ro/e denotes the ratio of observed to expected cell number. **(B)** FMO control for CD142 and a full stained sample from control group in flow cytometry. **(C)** Flow cytometry gating strategy and quantification of immune cells, NK cells, $CD4^+$T cells, $CD8^+$T cells and B cells in CAS (n = 14) v.s. control (n = 7) groups. **(D&E)** H&E staining morphology and quantification of PVAT comparing the control group (n = 15) with the CAS group (n = 87). Scale bar = 200 μm. **(F&G)** Sirius red staining morphology and quantification of PVAT comparing the control group (n = 15) with the CAS group (n = 87). Scale bar = 50 μm. Two-tailed unpaired t test was used for **(C)**, (**E**) and (**G**), with Welch's correction applied only to immune/NK/CD8+ T cells in **(C)**. Error bars show mean ± SD. Data in (A) presented as box and whiskers (box = 25^{th} -75^{th} percentile, line = median, and whiskers = 5^{th} -95^{th} percentile). Data are presented as individual samples in (A), (C), (E) and (G). CAS: carotid artery stenosis; PVAT: perivascular adipose tissue; ADSC: adipose-derived stem cell; UMAP: uniform manifold approximation and projection; FMO: fluorescence minus one. Source data are provided as a Source Data file.



Supplementary figure 3. Compositional shifts and functional heterogeneity of ADSC

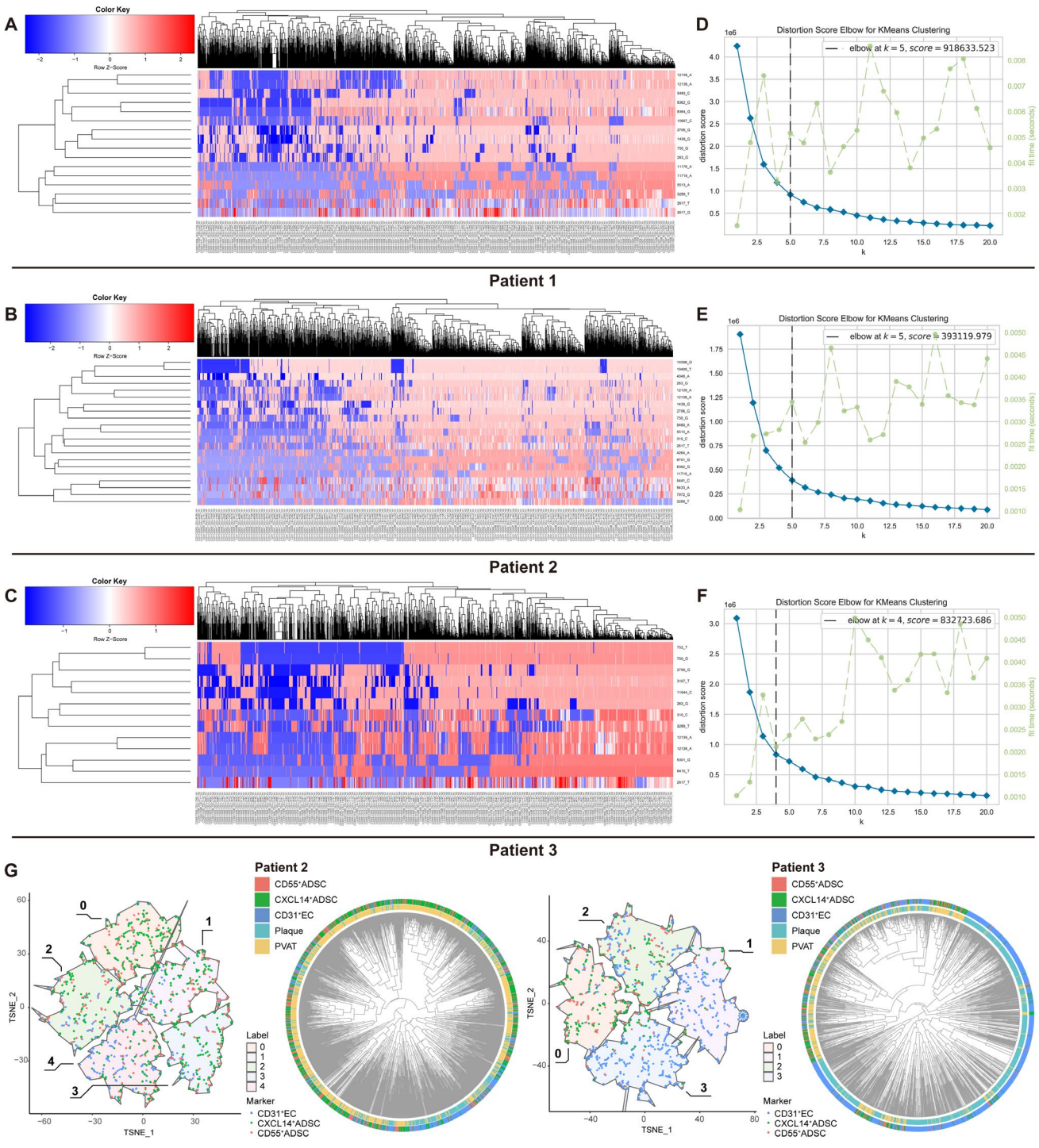
subpopulations in PVAT from patients with carotid atherosclerosis. (A) UMAP plot showing the unsupervised, low-dimensional embedding of ADSC subsets**. (B)** CXCL14 and CD55 expression defines distinct ADSC subpopulations. **(C)** Expression of CXCL14 and CD55 across unsupervised clustered ADSC subgroups. **(D)** Volcano plot of DEGs between $CD55^{+}$ADSC and $CXCL14^{+}$ADSC. **(E-I)** UMAP plots of the ADSC marker genes *CD34*, *ITGB1*, *F3* (CD142), *PDGFRA* and *PDGFRB*. **(J)** Immunofluorescence staining for CD142, PDGFRA, and PDGFRB in the perivascular adipose tissue of the carotid artery confirmed the co-localization of CD142 with classic mesenchymal stem cell markers. Immunofluorescence staining was repeated in 12 samples independently, and a representative image is shown. Scale bar = 100 μm. **(K)** UMAP plots of the $CXCL14^{+}$ADSC marker gene *GPC3*. **(L)** Immunofluorescence staining for CD142, CD55 and GPC3 in the perivascular adipose tissue of the carotid artery confirmed that CD55 and GPC3 can distinguish two distinct ADSC subpopulations. Immunofluorescence staining was repeated in 11 samples independently, and a representative image is shown. Scale bar = 100 μm. **(M)** Pseudotime analysis of the differentiation relationship between two ADSC subpopulations. **(N)** Cytotrace analysis of differentiation relationships among ADSC subsets. **(O)** Bubble plot of the expression patterns of positive chemotaxis and sprouting angiogenesis enrichment scoring-related genes within differentially expressed genes between $CXCL14^{+}$ADSC and $CD55^{+}$ADSC. **(P)** Immunofluorescence negative controls for Isolectin B4, CD142, CD55, GPC3 and CD31 in human carotid PVAT. Scale bar = 50 μm. **(Q)** Box plot of the proportion of $CD55^{+}$ADSC and $CXCL14^{+}$ADSC in the CAS (n = 6) and control (n = 2) groups (+, ++, +++; see Methods for Ro/e calculation). Samples with ≤10 cells were excluded. Data in (Q) presented as box and whiskers (box = 25^{th} -75^{th} percentile, line = median, and whiskers = 5^{th} -95^{th} percentile). Each point presented as an individual sample. DEG: differentially expressed gene; UMAP: uniform

manifold approximation and projection; PVAT: perivascular adipose tissue; ADSC: adipose-derived stem cell; CAS: carotid artery stenosis. Source data are provided as a Source Data file.



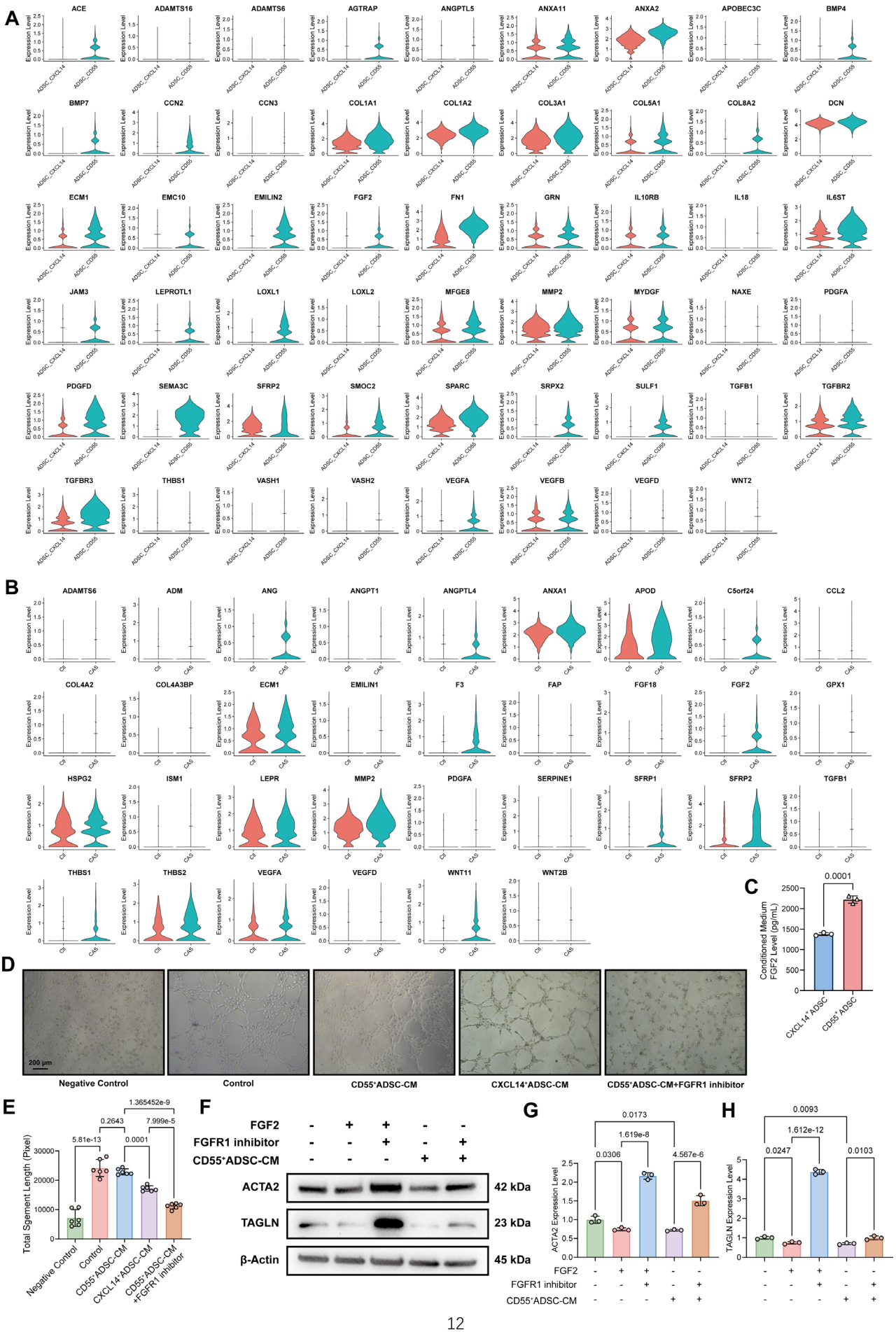
Supplementary figure 4. Functional characteristics and cellular heterogeneity of ADSCs in patients with carotid artery stenosis and mouse models. (A) Quantification of ADSC positive area

in asymptomatic (n = 40) vs. symptomatic (n = 49) CAS, and in those with (n = 31) v.s. without (n = 58) stroke history. **(B)** Representative immunofluorescence images of capillaries ($CD31^+$) in PVAT from CAS patients stratified by TIA symptoms and stroke history (n values as in A). Scale bar = 50 μm. **(C)** Expression levels of top 20 marker genes for $CD55^+$ADSC and $CXCL14^+$ADSC in coronary PVAT v.s. subcutaneous adipose tissue (GEO dataset GSE45169). Box plots show median, 25^{th}-75^{th} percentiles (box), and 5^{th}-95^{th} percentiles (whiskers). **(D)** Comparison of the expression pattern scores of marker genes between human-derived PVAT-ADSC subsets and mouse-derived PVAT-ADSC. **(E)** Evaluation of carotid artery remodeling in C57 mice using Oil Red O staining. **(F)** Western blot analysis of PDGFRA, PDGFRB and β-Actin expression in sorted human ADSC and HASMCs. **(G)** *In vivo* bioluminescence imaging of ADSC engraftment at the carotid ligation site in nude mice 28 days post-intervention. **(H)** Quantification of media remodeling in carotid arteries of nude mice across 8 sections spanning 1400 μm among $CXCL14^+$ADSC (n = 6), $CD55^+$ADSC (n = 5) and control group (n = 5). **(I)** Angiogenic capillary passing through the media and neointimal after ADSC intervention. Representative immunofluorescence image of angiogenic capillaries penetrating the media and neointima after ADSC intervention (n values as in H). Scale bar = 20 μm. **(J, K)** Mitochondrial lineage analysis of patient plaque samples by scRNA-seq. **(J)** UMAP projection identifying major plaque cell clusters. **(K)** Dot plot showing canonical marker expression for each major cell type. Two-tailed Mann Whitney test was used for analyses in (**A**). Two-tailed two-way ANOVA followed by Tukey's multiple comparisons test was used for analyses in (**H**). Data are presented as individual samples in **(A)** and **(H)**. Data are presented as the mean ± SD. * indicates p value < 0.05. ns: no significance; TIA: transient ischemic attack; ADSC: adipose-derived stem cell; HASMC: human aortic smooth muscle cell. Source data are provided as a Source Data file.

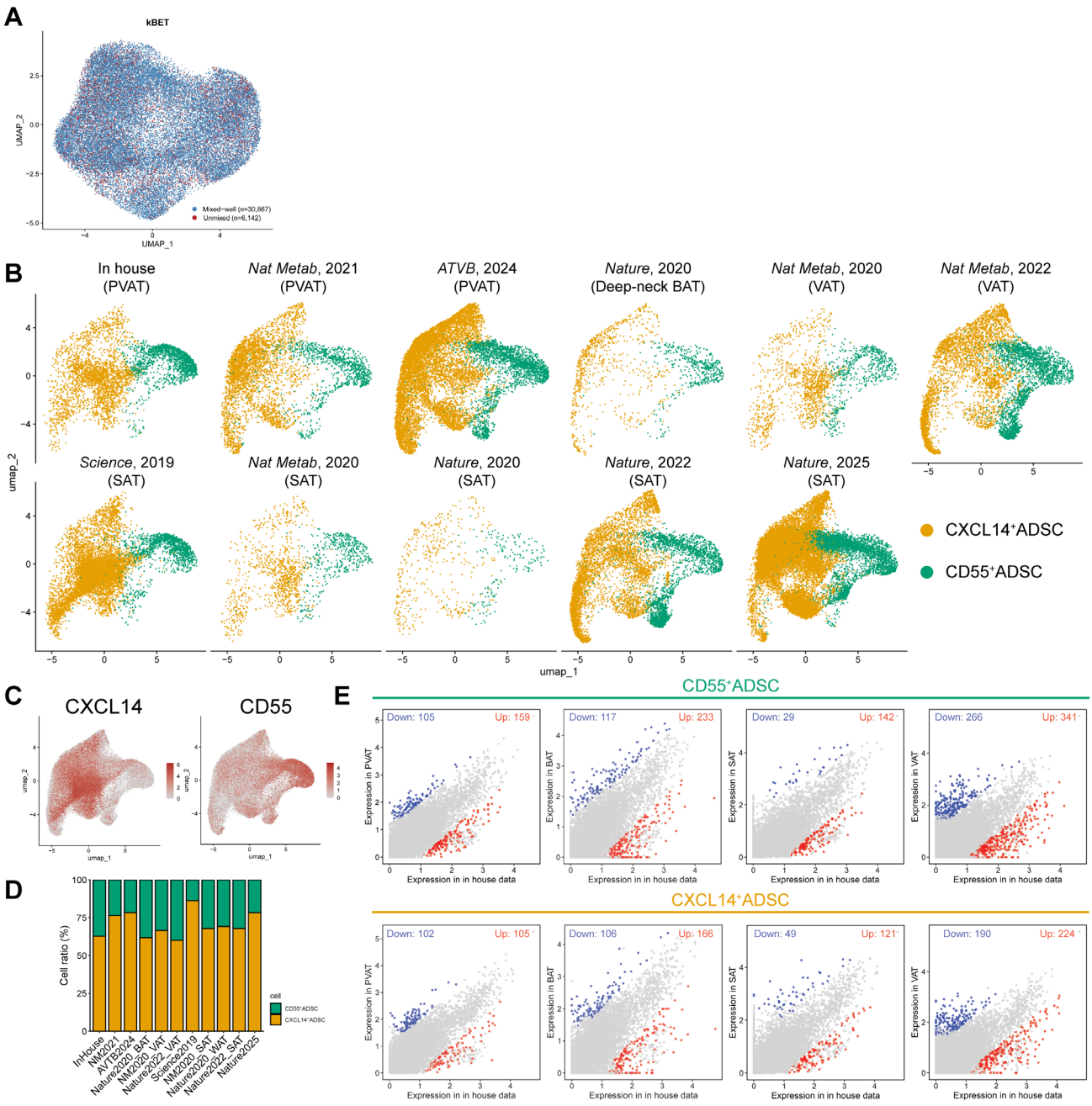


Supplementary figure 5. Mitochondrial lineage tracing reveals clonal relationships between PVAT-derived ADSC subtypes and plaque endothelial cells. (A-C) Hierarchical clustering mitochondrial genotyping profiles from $CD55^{+}$ADSC and $CXCL14^{+}$ADSC of PVAT to $CD31^{+}$endothelial cells of plaque. **(D-F)** Elbow plot depicting the optimal number of ADSC subtype

to $CD31^+$endothelial cell clone clusters based on mitochondrial genotyping profiles. The "elbow" point, where the curve flattens, indicates the optimal number of clusters. **(G)** t-SNE visualization and evolutionary tree of lineages from $CD55^+$ADSC and $CXCL14^+$ADSC of PVAT to $CD31^+$endothelial cells of plaque from the same patient. PVAT: perivascular adipose tissue; ADSC: adipose-derived stem cell. Source data are provided as a Source Data file.

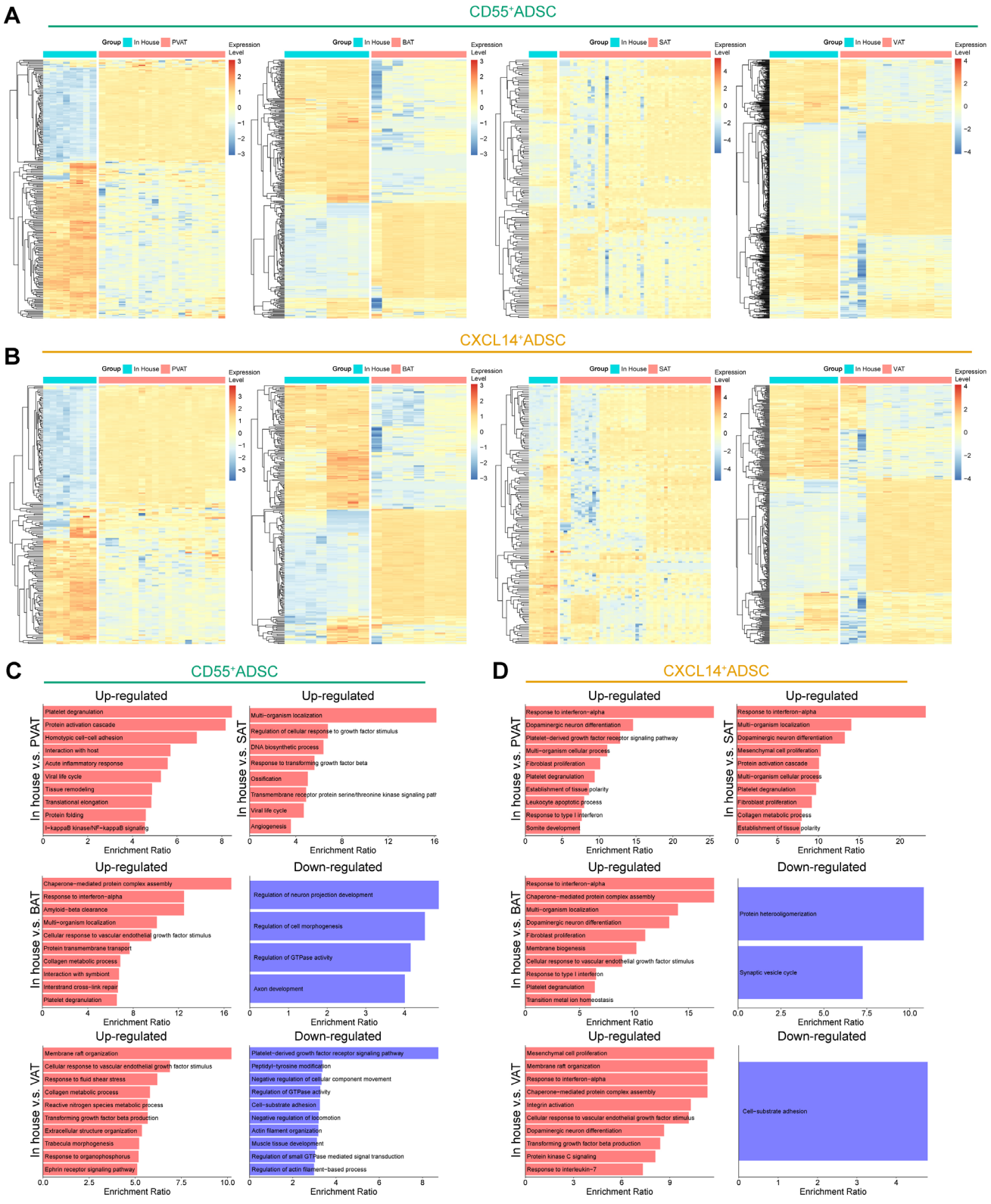

A
ACE
ADAMTS16
ADAMTS6
AGTRAP
ANGPTL5
ANXA11
ANXA2
APOBEC3C
BMP4
BMP7
CCN2
CCN3
COL1A1
COL1A2
COL3A1
COL5A1
COL8A2
DCN
ECM1
EMC10
EMILIN2
FGF2
FN1
GRN
IL10RB
IL18
IL6ST
JAM3
LEPROTL1
LOXL1
LOXL2
MFGE8
MMP2
MYDGF
NAXE
PDGFA
PDGFD
SEMA3C
SFRP2
SMOC2
SPARC
SRPX2
SULF1
TGFB1
TGFBR2
TGFBR3
THBS1
VASH1
VASH2
VEGFA
VEGFB
VEGFD
WNT2
Expression Level
ADSC_CXCL14
ADSC_CD55
B
ADAMTS6
ADM
ANG
ANGPT1
ANGPTL4
ANXA1
APOD
C5orf24
CCL2
COL4A2
COL4A3BP
ECM1
EMILIN1
F3
FAP
FGF18
FGF2
GPX1
HSPG2
ISM1
LEPR
MMP2
PDGFA
SERPINE1
SFRP1
SFRP2
TGFB1
THBS1
THBS2
VEGFA
VEGFD
WNT11
WNT2B
Ctl
CAS
C
Conditioned Medium FGF2 Level (pg/mL)
0.0001
CXCL14+ADSC
CD55+ADSC
D
200 μm
Negative Control
Control
CD55+ADSC-CM
CXCL14+ADSC-CM
CD55+ADSC-CM+FGFR1 inhibitor
E
Total Sgement Length (Pixel)
1.365452e-9
0.2643
7.999e-5
5.81e-13
0.0001
Negative Control
Control
CD55+ADSC-CM
CXCL14+ADSC-CM
CD55+ADSC-CM +FGFR1 inhibitor
F
FGF2
FGFR1 inhibitor
CD55+ADSC-CM
ACTA2
TAGLN
β-Actin
42 kDa
23 kDa
45 kDa
G
0.0173
1.619e-8
0.0306
4.567e-6
ACTA2 Expression Level
FGF2
FGFR1 inhibitor
CD55+ADSC-CM
H
0.0093
1.612e-12
0.0247
0.0103
TAGLN Expression Level

Supplementary figure 6. CD55$^+$ADSC-secreted FGF2 promotes angiogenesis and smooth muscle cell phenotypic switching via the FGF2–FGFR1 signaling pathway. (A-B) Genes that belong to the GOBP VASCULATURE DEVELOPMENT gene set and encode secreted proteins. Within this predefined space, we compared genes that were upregulated in CD55+ADSC relative to CXCL14+ADSC (A), as well as genes that were upregulated in CD55+ADSC (CAS condition) compared with the control group (B). **(C)** ELISA test detecting the expression level of FGF2 in ADSC-conditioned medium. Experiments were performed with three biological replicates. **(D-E)** Representative images (D) and statistical analysis (E) of the HUVEC tube formation assay, examining whether CD55$^+$ADSCs promote angiogenesis via the FGF2–FGFR1 pathway. FGFR1 inhibitor (PD173074, 25 nM). Experiments were performed with six biological replicates. Scale bar = 200 μm. **(F-H)** Western blot band images (F) and statistical analysis of ACTA2 (G), TAGLN (H) and β-Actin expression in HASMCs following treatment with ADSC-conditioned medium (CM), FGF2 (25 ng/mL), and FGFR1 inhibitor (PD173074, 10 nM), to assess the role of the FGF2-FGFR1 pathway in promoting smooth muscle cell phenotypic switching. Experiments were performed with three biological replicates. Data are presented as the mean ± SD. Two-tailed unpaired t-test was used for analyses in (**C**). Two-tailed one-way ANOVA followed by Tukey's multiple comparisons test was used for analyses in (**E**), (**G**) and (**H**). CAS: carotid artery stenosis; ADSC: adipose-derived stem cell; HUVEC: human umbilical vein endothelial cell; CM: conditioned medium; HASMC: human aortic smooth muscle cell. Source data are provided as a Source Data file.



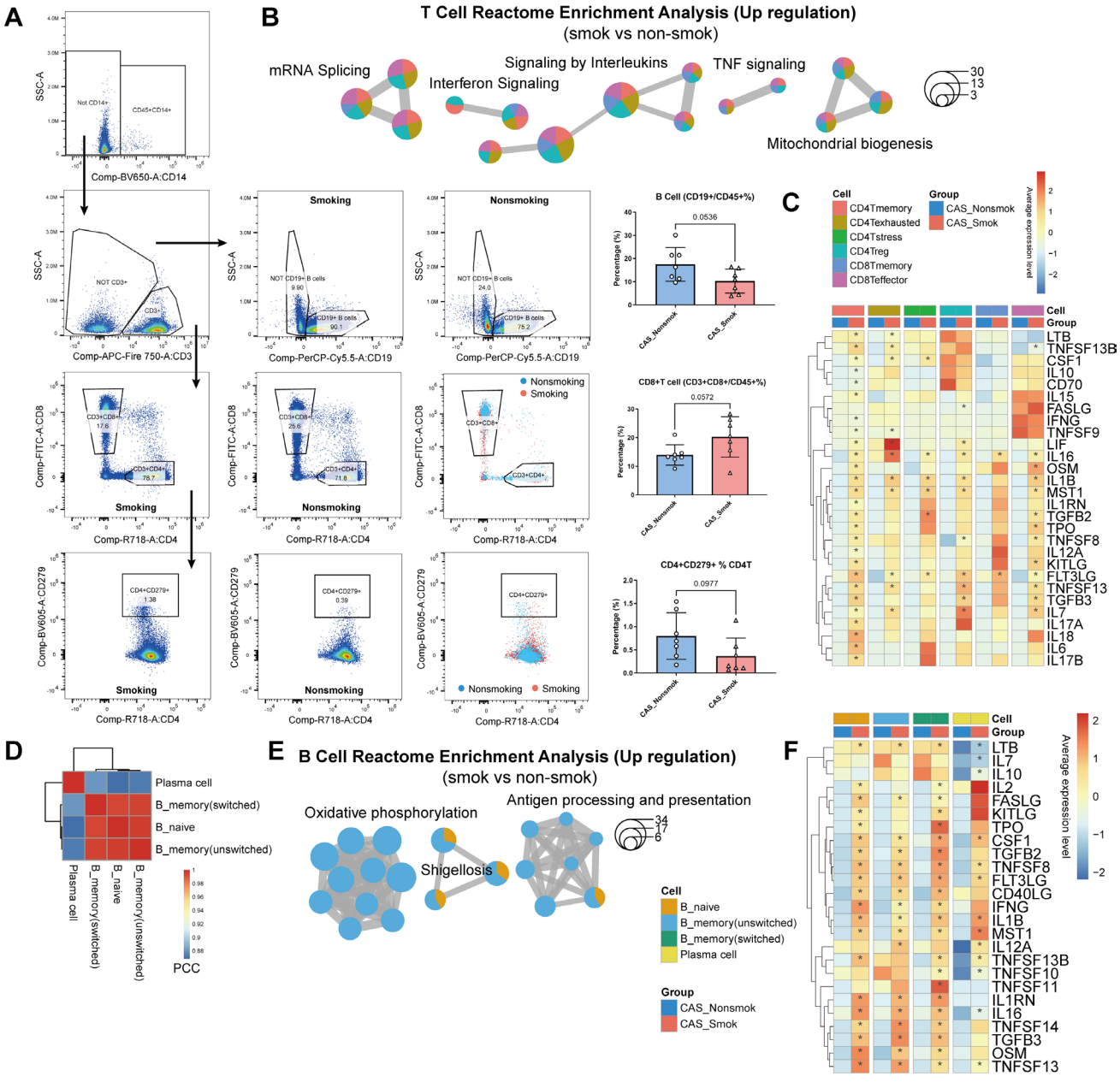
Supplementary figure 7. Comparative analysis of ADSCs across single-cell datasets from different adipose depots. (A) UMAP plot shows cells colored by kBET result after combining in-house ADSCs with public adipose tissue datasets. **(B)** UMAP plot showing the distribution and integration of ADSCs from our in-house dataset with public PVAT, deep-neck BAT, SAT, and VAT datasets. **(C)** UMAP visualization of CXCL14 and CD55 expression in ADSCs across all integrated datasets. **(D)** Bar plot comparing the proportions of CD55⁺ADSC and CXCL14⁺ADSC subpopulations

among datasets. **(E)** Volcano plots of differentially expressed genes (DEGs) between $CD55^{+}$ADSCs and $CXCL14^{+}$ADSCs in the in-house dataset compared separately to PVAT, deep-neck BAT, SAT, and VAT datasets. DEG: differentially expressed genes; PVAT: Perivascular adipose tissue; SAT: Subcutaneous adipose tissue; VAT: Visceral adipose tissue; BAT: Brown adipose tissue; WAT: White adipose tissue; ADSC: Adipose-derived stem cells. Source data are provided as a Source Data file.



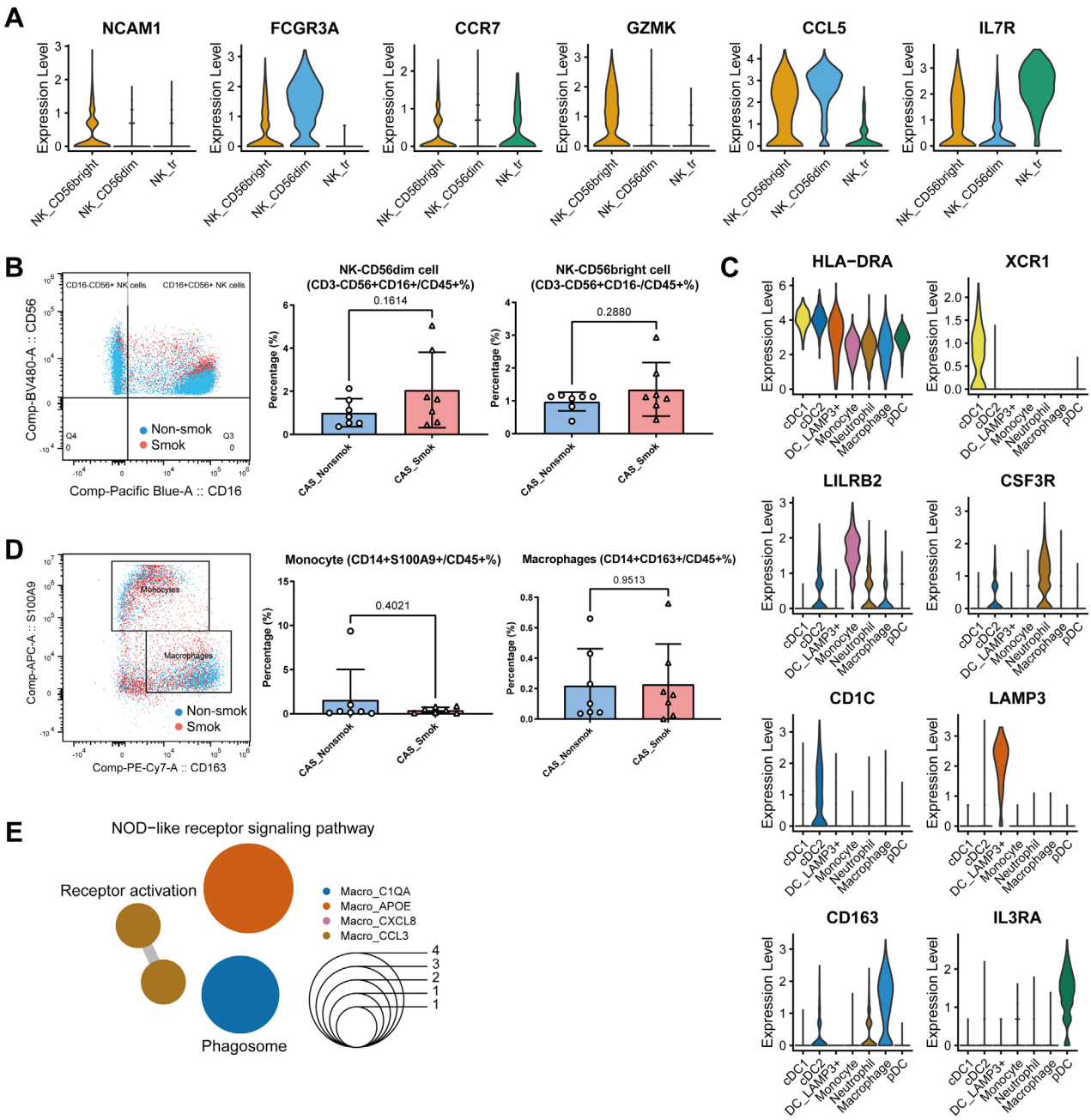
Supplementary figure 8. Transcriptomic comparison of PVAT-derived ADSC subtypes across multiple adipose depots reveals depot-specific gene expression and functional enrichment profiles. (A-B) Heatmaps showing the DEGs for CD55^{+}ADSCs (A) and CXCL14^{+}ADSCs (B) from

our in-house dataset against public PVAT, deep-neck BAT, SAT, and VAT datasets. **(C-D)** Bar charts display enriched functions for genes up-regulated (red) or down-regulated (blue) in CD55^{+}ADSCs **(C)** and CXCL14^{+}ADSCs **(D)** across the four adipose depot comparisons. DEG: differentially expressed genes; PVAT: Perivascular adipose tissue; SAT: Subcutaneous adipose tissue; VAT: Visceral adipose tissue; BAT: Brown adipose tissue; WAT: White adipose tissue; ADSC: Adipose-derived stem cells. Source data are provided as a Source Data file.



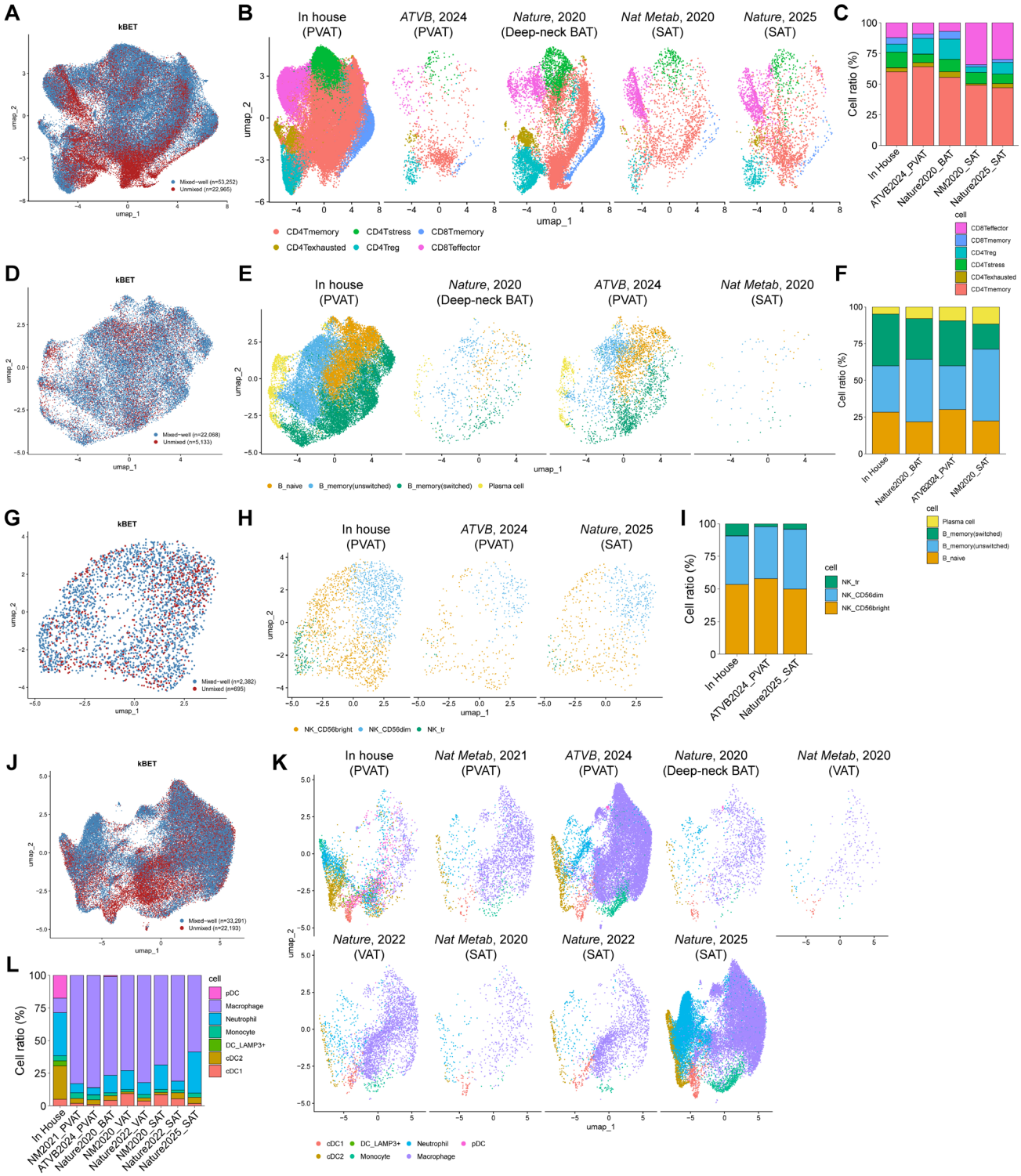
Supplementary figure 9. Smoking-associated immune dysregulation in T and B cell

subpopulations in carotid artery stenosis patients. (A) Flow cytometry gating strategy and quantification of CD4Texhausted (CD4-CD279-) and CD8Teffector (CD8+CD74+) cells in smoking (n=7) v.s. non-smoking (n=7) CAS groups. **(B)** Functional enrichment analysis of upregulated DEGs in T cell subpopulations in smoking v.s. non-smoking CAS groups. **(C)** Cytokine expression of T cell subclusters in smoking v.s. non-smoking CAS groups. The color bar represents the average expression level of cytokines in corresponding T cell subclusters. **(D)** Correlation heatmap of B cell subclusters. The color bar represents the Pearson correlation coefficient (PCC). **(E)** Functional enrichment analysis of upregulated DEGs in B cell subpopulations in smoking v.s. non-smoking CAS groups. **(F)** Cytokine expression of B cell subclusters in smoking v.s. non-smoking CAS groups. The color bar represents the average expression level of cytokines in corresponding B cell subclusters. Two-tailed unpaired t test was used for **(A)**. Data are presented as individual samples in **(A)**. Data are presented as the mean ± SD. CAS: carotid artery stenosis; DEG: differentially expressed gene; ADSC: adipose-derived stem cell; PCC: Pearson correlation coefficient. Source data are provided as a Source Data file.



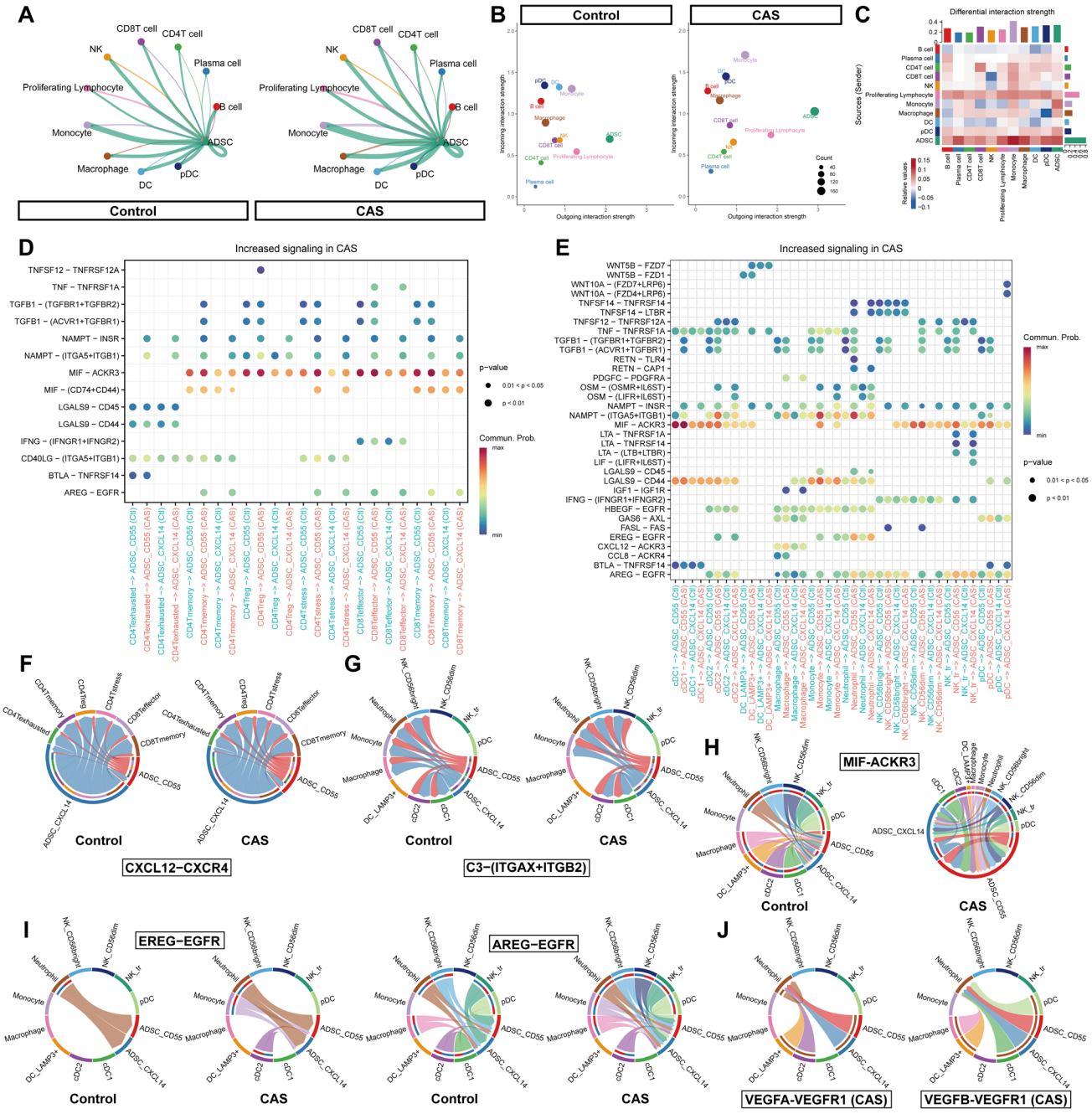
Supplementary figure 10. Characterization of NK cell and myeloid cell subpopulations and their smoking-associated alterations in carotid artery stenosis patients. **(A)** Violin plot of the expression of canonical markers for NK cell subtypes. **(B)** Flow cytometry gating strategy and quantification of NK_CD56dim (CD56 low+CD16+) and NK_CD56bright (CD56+CD16-) cells in smoking (n=7) v.s. non-smoking (n=7) CAS groups. **(C)** Violin plot of the expression of canonical markers for major myeloid cell subtypes. **(D)** Flow cytometry gating strategy and quantification of macrophages and

monocytes in smoking (n=7) v.s. non-smoking (n=7) CAS groups. **(E)** Functional enrichment analysis of upregulated DEGs in macrophage subpopulations in CAS patients. Data are presented as individual samples in **(B)** and **(D)**. Data are presented as the mean ± SD. Two-tailed unpaired t test and Two-tailed unpaired t test with Welch's correction were used for (**B**) and (**D**). CAS: carotid artery stenosis; NK: natural killer; DEG: differentially expressed gene; ADSC: adipose-derived stem cell. Source data are provided as a Source Data file.



Supplementary figure 11. Comparative analysis of immune cells across single-cell datasets from different adipose depots. (A) UMAP plot shows cells colored by kBET result after combining in-house T cells with public adipose tissue datasets. **(B)** UMAP plot showing the distribution and integration of CD4/CD8 Tmemory cell, Treg cell, CD8effector cells from our in-house dataset with

public PVAT, BAT and SAT datasets. **(C)** Bar plot comparing the proportions of CD4/CD8 Tmemory cell, Treg cell, CD8effector cells among datasets. **(D)** UMAP plot shows cells colored by kBET result after combining in-house B cells with public adipose tissue datasets. **(E)** UMAP plot showing the distribution and integration of B_naive, B_memory(unswitched), B_memory(switched) and plasma cells from our in-house dataset with public PVAT, BAT and SAT datasets. **(F)** Bar plot comparing the proportions of B_naive, B_memory(unswitched), B_memory(switched) and plasma cells among datasets. **(G)** UMAP plot shows cells colored by kBET result after combining in-house NK cells with public adipose tissue datasets. **(H)** UMAP plot showing the distribution and integration of NK_tr, NK_CD56dim and NK_CD56bright cells from our in-house dataset with public PVAT datasets. **(I)** Bar plot comparing the proportions of NK_tr, NK_CD56dim and NK_CD56bright cells among datasets. **(J)** UMAP plot shows cells colored by kBET result after combining in-house DC cells with public adipose tissue datasets. **(K)** UMAP plot showing the distribution and integration of macrophage, neutrophil/monocyte, cDC1, cDC2, DC_LAMP3+ and pDCs from our in-house dataset with public PVAT, SAT and BAT datasets. **(L)** Bar plot comparing the proportions of macrophage, neutrophil/monocyte, cDC1, cDC2, DC_LAMP3+ and pDC cells among datasets. PVAT: Perivascular adipose tissue; SAT: Subcutaneous adipose tissue; VAT: Visceral adipose tissue; BAT: Brown adipose tissue; WAT: White adipose tissue. Source data are provided as a Source Data file.



Supplementary figure 12. Enhanced intercellular communication networks between ADSC subtypes and immune cell populations in carotid artery stenosis. (A) Cell-cell crosstalk analysis depicting major cell type interaction weights in control v.s. CAS groups. **(B)** Outgoing-Incoming interaction strength analysis among major cell types in control v.s. CAS groups. (**C**) Interaction strength difference analysis among major cell types in control v.s. CAS groups. **(D)** Ligand-receptor bubble plot of increased communication from T cell subpopulations to ADSC subtypes. **(E)** Ligand-

receptor bubble plot of increased communication from myeloid subtypes to ADSC subtypes. (**F-J**) Chordal chart of CXCL12-CXCR4, C3-(ITGAX+ITGB2), MIF-ACKR3, EREG-EGFR, AREG-EGFR, VEGFA-VEGFR1 and VEGFB-VEGFR1 pathway communication strength among ADSC subtypes, T cell subtypes, NK cell subtypes and myeloid cell subtypes in CAS group and/or control group. CAS: carotid artery stenosis; ADSC: adipose-derived stem cell. Source data are provided as a Source Data file.